Small-Signal Stability Assessment of the Cameroonian Southern Interconnected Grid

Jules Tsochounie[1], Emmanuel Tanyi[2], Daniel Tchiotsop[3]

[1,3]Department of Electrical Engineering, IUT FOTSO Victor, University of Dschang, BP 134 BANDJOUN
[1]jtsoch@yahoo.fr, [3]dtchiotsop@yahoo.fr
[2]Department of Electrical and Telecommunications Engineering, ENSPY, University of Yaounde 1
emmantanyi@yahoo.com

Abstract— *This article investigates the performance of the generator excitation loop equipped with a PID controlled AVR system, and of the dam automaton consisting of a PID controlled water flow regulation system in the southern interconnected grid (SIG) of the Cameroonian power system, when subjected to small perturbations, using linearized state-space models of the power plant. A fifth order model of the synchronous generator with a high gain excitation system and AVR is considered. A detailed formulation of equations comprising the mechanical and electrical swing dynamics of the turbine-generator unit and the load is realized; a multivariable state-space non linear model of the one area single machine system model is obtained. For small-signal performance analysis, the model is linearized around an operating point. The article also presents a state-space model of the water flow system. The effects of PID controlled AVR and water flow regulation systems are examined through performing of extensive MATLAB simulations to analyze the behavior of the proposed models following small disturbances. The simulation results presented in this paper are obtained using a MATLAB computer program developped by the authors; they provide useful insight into the dynamic behavior of the Cameroonian SIG, including stability, speed of response and steady-state accuracy. The paper establishes that the classical control systems do not have very good performance: long settling time, high overshoot, relativly slow response, and many damped oscillations.*

Keywords— AVR, excitation system, PID controller, state-space modeling, small-signal stability.

I. INTRODUCTION

Stability is one of the important issues of safe power system operation. Repeated global power outages due to power system instability reveal the importance of the issue [1]. Power system oscillations were first observed as soon as two or more synchronous generators were connected together to provide more generation capacity and reliability. Originally, the fairly closely connected synchronous generators were observed to swing against each other at low frequency; these spontaneous oscillations appeared in mechanical variables like rotor angle and speed [2]. Since synchronous generators are rotating electromechanical devices, mechanical oscillations of their rotor were transmitted by electromagnetic induction to electrical variables like bus voltages, line currents and power. The oscillations are initiated by variations in generation and custom loads, which act upon the systems as perturbations or disturbances. Because power systems have an almost continuously time varying nature – load and thus power demand vary in time, they always suffer from oscillations. Power system oscillations are therefore inevitable and are a characteristic of the system. The perturbations could be normal or abnormal. Normal perturbations are often of small magnitude, and abnormal perturbations like loss of a large generator or custom load, and short-circuit on a transmission line or in a substation are of large magnitude. Power system oscillations become much worse following a large disturbance. In some cases the low frequency growing oscillations cause loss of power supply to custom loads, loss of synchronism among generators, or they reduce transmission capability of long transmission lines; these are expressions of power system instability. Voltage oscillations in a power system indicate a high degree of its vulnerability, because a change in the condition of power system could easily lead to a progressive drop in voltage at all buses in the transmission network, and to voltage collapse. Distribution networks are practically exempted from this problem due to their passive nature. Over the last three decades, the problems of low frequency oscillations in power systems have assumed importance.

The stability issue of power systems can thus be stated in three aspects [3], [4]: (i) rotor (or power) angle stability, (ii) bus voltage stability and (iii) frequency stability. An upset in the balance between power generation and power demand can affect frequency stability; the frequency could no more be maintained within the stability limits. The inability of the power system to meet the demand for reactive power causes voltage instability. However, voltage instability does not always occur alone; often angle and voltage instabilities are associated. One may lead to the other and the distinction may not be clear.

Moreover, as power systems are nonlinear, their stability depends on both the initial conditions and the magnitude of a disturbance. Consequently, rotor angle and voltage stability can be divided into steady-state or small-signal stability and transient or large disturbance stability [1], [5]. A distinction between these two types of stability is important for understanding the underlying causes of the problems in order to develop appropriate controls and operating procedures. Under steady-state operating conditions, bus voltages and line currents of all the synchronous generators must have the same frequency and the rotor mechanical speed of each generator must be synchronized to this frequency: the generators are said to operate in synchronism. A perturbation on the power system that results in a change of the electrical torque could cause oscillations of the generator rotor around its equilibrium point due to insufficient damping torque component, or a steady increase in the rotor angle due to insufficient synchronizing torque component. A high magnitude of rotor oscillations or the angle drift of the generator rotor can entail loss of synchronism with the rest of the network and disconnection of certain generators; rotor angle instability is associated with slow loss of synchronism among generators.

In the Cameroonian power system, considering the southern interconnected grid (SIG) consisting of two hydropower plants with 16 turbine-generator units and one gas plant, which supplies six regions of the country where almost 90% of economic and industrial activity in the country is concentrated, it constitutes the core of the Cameroonian power system, and provides the bulk of Cameroons' electricity [6]. In the SIG, power generation is centralized and hydro-dominant; the three power generating stations are connected to a very high voltage transmission substation in Mangombe, and from there power is transmitted to the different load centers. In the past two decades the SIG suffered from instability which prevented the grid from beeing fully utilized, and from very poor power quality; it experienced many perturbations due to power imbalance – insufficient power generation and increased active or reactive power demand. Low frequency oscillations were observed in bus voltages and line currents; they often caused loss of power supply to custom loads in the nearby region, or reduced power transmission capability of long transmission lines like those from Mangombe to Yaounde and Bafoussam. The transmission network in the SIG also often experienced voltage drops and voltage oscillations during periods of high power demand. During dry seasons, perturbations were worsened due to insufficient water flow for production; power furniture could not meet demand and was frequently interrupted for hours or days – load shedding was often used to match power demand with power production.

In power systems, a particular issue encountered at the generating plant level is to maintain stability under various operating conditions [3]. The problem of small-signal stability in generating plants is usually one of insufficient damping of their oscillations. The first solution to this problem was to realize damper windings on generators and turbines [7]. But with generators equipped with slow excitation systems (DC and AC excitations), the available synchronizing torque was weak. This weakness of the synchronizing torque was found to be causing system instability when power systems started operating close to their stability limits. To enhance the synchronizing torque, fast excitation systems (static excitations) were used [5]. To avoid this second problem, an automatic voltage regulator (AVR) was installed on the generators, so that it acted on their excitation system. The generator control is one of the basic control means of power systems; it incorporates also a speed governor for speed control. The AVR introduces a positive synchronizing torque component in excitation systems, and a negative damping torque component that reduces the damping of the system oscillations [3]. A poorly damped power system could be subjected to cascade failure after a variation of demand. The low frequency oscillations in power plants incorporating generators equipped with a static excitation system were traced to fast voltage regulation. The generators of the Song-Loulou power plant are equipped with static excitation systems; thus there is a risk that by greater amounts of power flowing across High Voltage or Very High Voltage long transmission lines an increasingly nefarious oscillatory instability factor be added compared to earlier situations, leading to low frequency oscillations in the SIG.

To enhance the stability of power systems, Power System Stabilizers (PSSs) and Flexible Alternating Current Transmission Systems (FACTS) are being currently used as additional controllers. Although FACTS are quite effective on damping low frequency oscillations, they are merely used to enhance the capability of transmission lines, but they are not used in the SIG. The PSS is added to the AVR in the generator excitation system to enhance the damping of low frequency small-signal oscillations. The operation of the Cameroonian SIG equipped with classical AVR and PSS has been shown to be unsatisfactorily. Experience has shown that a classical power system stabilizer tuned for an operating point do not show good performance by perturbations in different operating points [8]. There is need for additional generator controllers which simultaneously increase the damping of power system oscillations and the synchronizing torque, in order to enhance the overall steady-state and dynamic stability (angle, voltage, and frequency) of the Cameroonian SIG.

Modern control theory with multivariate approach could offer some tools for this task. Until now, from the existing generator control systems none is the implementation of modern control theory [9], they were designed using frequency or root locus method, and they were designed to solve a single problem. It was seen that they helped solve one aspect of the problem, but to the detriment of another aspect. Control system design generally begins with the realization of an appropriate model for the dynamic system, which will be used to evaluate its overall performances. Power system operators and planners need effective tools to assess the overall stability of the system and take appropriate actions to enhance its stability over a wide range of operating conditions: the model simulation. Modeling of power plants and their loads is therefore fundamental to the evaluation of their performance by simulation and design of their control.

Numerous research works have been done and published on modeling and simulation of power systems for small-signal stability studies. Demello and Concordia [4], Kundur et al. [11], and Chow et al. [12] developed a linearized model of synchronous generator and its excitation system connected to an infinite bus in the form of block diagram, in frequency domain. Baghani and Koochaki [8] developed a linearized state-space model of a synchronous generator and its excitation system. Their model was derived from the steady-state harmonic operation which is linear. Pedro Camilo de Oliveira e Silva et al. [13] developed a linearized state-space model of a complete power plant.

For the Cameroonian SIG, state-space models of water flow system, turbine-generator unit, voltage control system, speed control system, and load connected at the generator terminals will be developed. Thank to the architecture of the SIG that is rather a radial than a meshed one, the SIG can be considered as simple, and will be modeled as a one area single machine system. The model must overcome some of the shortcomings of the aforementioned models. Thus, the turbine-generator unit model will be built by physical principles and put in state-space form. Small disturbances hypothesis permits the linearization of the system of equations and the application of all the wealth of the modern control theory. The other devices will be transformed from frequency representation form that is already linear, into state-space representation form. The performance of the integrated overall system will be assessed using MATLAB simulation.

The rest of this paper is structured as follows: in section II the feedback control structure of the system is presented. In section III the detailed development of a linearized state-space model of the Cameroon SIG is realized; this linearized form is suitable for practical study of the classical control systems performance. Some illustrative simulation results are presented and discussed in section IV. In the final section of the paper some concluding remarks are mentioned.

II. FEEDBACK CONTROL STRUCTURE OF THE POWER SYSTEM

The Cameroonian SIG incorporates in reality many autonomous feedback control systems, each consisting of a generating unit (turbine and alternator), and the load. It can be modeled as a one area single machine system.

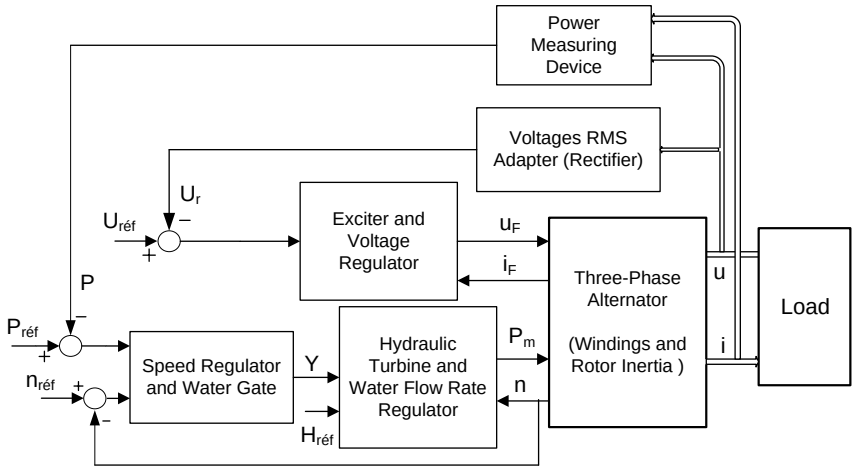

FIG. 1: FEEDBACK CONTROL STRUCTURE OF THE POWER PLANT

The structure of the feedback control system of the SIG is shown in fig. 1 [14]. A generating unit incorporates three feedback control loops for the regulation of the three main variables influencing the power output. These variables include the flow rate of water impacting the turbine, the alternator rotor speed and the alternator armature voltage which determines the magnetic flux permeating the armature circuit. Each of these variables is maintained at a reference value by an appropriate feedback control loop.

III. STATE-SPACE MODELING OF THE POWER SYSTEM

3.1 The Turbine-Alternator Sub-system

From a system dynamics perspective, the alternator is the most complex component of the power system, due to the presence of several coils in armature and in rotor, which are mounted on separate geometrical axis and are magnetically mutually coupled. The alternators used in hydro electric power generating plants are salient poles synchronous machines. Their permeance varies across the air gap with respect to the pole axis (d-axis) of the polar wheel and to an axis at right angle to the pole axis, the quadrature axis (q-axis) [14]. As a logical consequence of this, an orthogonal system with **d-q** axis is introduced on the rotor, with the d-axis superimposed on the polar axis and the q-axis lagging the d-axis. The various inductances in the alternator are represented by six coils [3], [15]. The stator contains three coils mounted on three axis separated from each other by an angle of 120°. The inductor coil **F** is located on the rotor in the d-axis. The damping effect is represented by the short-circuited fictitious coils **KD** and **KQ** in the d- and q-axis respectively. Some inductances vary with the angular position of rotor with respect to the axis of armature reference coil θ which in turn varies with time. This introduces considerable complexity in the machine differential equations whose coefficients are time variable. The elimination of the time dependency of the inductance terms is obtained by Park's transformation [15]. Due to this transformation, the magnetizing effect of the three-phase armature currents is replaced by that of their components $i_d(t)$ and $i_q(t)$ flowing in two imaginary coils located on the **d-** and **q-**axis of the rotor, and the magnetizing effect of the damping coils is due to the currents $i_{KD}(t)$ and $i_{KQ}(t)$ flowing in coils **KD** and **KQ**.

3.1.1 Electrical State-Space Model of the Alternator

The electrical state-space model of the three phase alternator in d-q-0 components is [14]:

$$\begin{pmatrix} \frac{di_d(t)}{dt} \\ \frac{di_q(t)}{dt} \\ \frac{di_F(t)}{dt} \\ \frac{di_{KD}(t)}{dt} \\ \frac{di_{KQ}(t)}{dt} \end{pmatrix} = \left[A'_G\right] \cdot \begin{pmatrix} i_d(t) \\ i_q(t) \\ i_F(t) \\ i_{KD}(t) \\ i_{KQ}(t) \end{pmatrix} + \left[B'_G\right] \cdot \begin{pmatrix} -u_d(t) \\ -u_q(t) \\ u_F(t) \\ 0 \end{pmatrix} \quad (1)$$

where the zero-sequence voltage u_0 and current i_0 are zero, since the alternator operation is assumed to be in equilibrium. The system matrices $\left[A'_G\right]$ and $\left[B'_G\right]$ are independent of time and are defined in Appendix 1.

3.1.2 Mechanical model of the Rotor of Alternator-Turbine Unit

Assuming rigid coupling of turbine and alternator, the motion of the rotor is described by the following equation:

$$J_t \frac{d^2\theta_m}{dt^2} = T_m - T_{em} \quad (2)$$

where,

J_t = moment of inertia of all rotating elements
T_m = mechanical torque produced by the turbine
T_{em} = electrical torque opposing the motion of the rotor
θ_m = mechanical angle

In the Park transformed electrical model of the generator, the electromagnetic torque results from the interaction between the total flux linkages Ψ_d and Ψ_q with the fictitious windings in d- and q-axis, and the currents through these windings i_d and i_q. It is expressed as follows [14], [15]:

$$T_{em} = p \cdot \left(\Psi_d \cdot i_q - \Psi_q \cdot i_d \right) \tag{3}$$

where,

Ψ_d and Ψ_q = fluxes permeating the coils **d** and **q**, respectively

i_d and i_q = currents in the coils

p = number of pairs of poles

The expressions of Ψ_d and Ψ_q are given by [14], [15]:

$$\begin{cases} \Psi_d(t) = L_d\, i_d(t) + \sqrt{\frac{3}{2}} M_{FS}\, i_F(t) + \sqrt{\frac{3}{2}} M_{KD,S}\, i_{KD}(t) \\ \Psi_q(t) = L_q\, i_q(t) + \sqrt{\frac{3}{2}} M_{KQ,S}\, i_{KQ}(t) \end{cases} \tag{4}$$

The electromagnetic torque then has the detailed form:

$$T_{em} = p\left\{ \left(L_d - L_q \right) i_d\, i_q + \sqrt{\frac{3}{2}} M_{FS}\, i_q\, i_F \right\} + p\left\{ \sqrt{\frac{3}{2}} M_{KD,S}\, i_q\, i_{KD} - \sqrt{\frac{3}{2}} M_{KQ,S}\, i_d\, i_{KQ} \right\} \tag{5}$$

Even at synchronous speed, the rotor oscillates and EMFs are then induced in the damping coils and in the rotor iron. The currents driven by the induced EMFs (eddy currents in the rotor iron) interact with the flux linkages of the damping coils and produce a torque which dampens the oscillations (Lenz's law). The effects of eddy-currents in the rotor iron and of currents in the damper coils can be lumped into a damping torque. The second term in equation (5) is obviously the damping torque T_D which is moreover proportional to the rate of change of the angle of polar wheel. It is described by the equation:

$$T_D = p\left\{ \sqrt{\frac{3}{2}} M_{KD,S}\, i_q\, i_{KD} + \sqrt{\frac{3}{2}} M_{KQ,S}\, i_d\, i_{KQ} \right\} = k_D \frac{d\delta_p}{dt} \tag{6}$$

Substituting for T_{em} and T_D in equation (2) results in the non-linear differential equation that describes the mechanical behavior of the generator rotor and the turbine:

$$\frac{d\dot{\delta}_p}{dt} + \frac{p\, k_D}{J_t} \frac{d\delta_p}{dt} = \frac{p}{J_t} T_m - \frac{p^2}{J_t} \left(L_d - L_q \right) i_d\, i_q - \frac{p^2}{J_t} \sqrt{\frac{3}{2}} M_{FS} i_q\, i_F \tag{7}$$

where $\frac{d^2\theta}{dt^2} = \frac{d^2\delta_p}{dt^2} = \frac{d\dot{\delta}_p}{dt}$.

3.1.3 Linearization of the mechanical model

During stable and balanced operation of the alternator, the stator phase voltages are sinusoïdal of constant magnitude $\hat{V}$, they form a balanced three phase system. Applying the inverse Park transform to the system of phase voltages results in the components [14] :

$$\begin{cases} u_d(t) = -\sqrt{3} V \sin \delta_p = -U \sin \delta_p \\ u_q(t) = \sqrt{3} V \cos \delta_p = U \cos \delta_p \end{cases} \tag{8}$$

When the system oscillates about an operating point (u_{d0}, u_{q0}, U_0, δ_{p0}) with the small variations ΔU and $\Delta\delta_p$ of the variables U and δ_p respectively, the small variations of the components u_d and u_q can be approximated as:

$$\begin{aligned} \Delta u_d &\approx -\sin \delta_{p0}\, \Delta U - \left(U_0 \cos \delta_{p0} \right) \Delta\delta_p \\ \Delta u_q &\approx \cos \delta_{p0}\, \Delta U - \left(U_0 \sin \delta_{p0} \right) \Delta\delta_p \end{aligned} \tag{9}$$

Linearising equation (1) and ignoring the damping currents i_{KD} and i_{KQ} whose effect has already been taken into account by introduction of the damping torque T_D, results in the following state equations of the three phase alternator:

$$\begin{pmatrix} \frac{d\Delta i_d}{dt} \\ \frac{d\Delta i_q}{dt} \\ \frac{d\Delta i_F}{dt} \end{pmatrix} = [A_G] \cdot \begin{pmatrix} \Delta i_d \\ \Delta i_q \\ \Delta i_F \end{pmatrix} + [B_G] \cdot \begin{pmatrix} \Delta U \\ \Delta \delta_p \\ \Delta u_F \end{pmatrix} \tag{10}$$

where the system matrices $[A_G]$ and $[B_G]$ are given in appendix 1. Equation (7) can also be linearized by considering small variations about an operating point (i_{d0}, i_{q0}, i_{F0}, n_0, T_{m0}, P_{m0}). The linearized version of this equation is of the form :

$$\begin{aligned} \frac{d\Delta\dot{\delta}_p}{dt} + \frac{p\,k_D}{J_t}\frac{d\Delta\delta_p}{dt} = &-\frac{p^2}{J_t}\left(L_d - L_q\right) i_{q0}\Delta i_d - \frac{p^2}{J_t}\left(\left(L_d - L_q\right) i_{d0} + \sqrt{\frac{3}{2}} M_{FS} i_{F0}\right)\Delta i_q - \\ &- \frac{p^2}{J_t}\sqrt{\frac{3}{2}} M_{FS} i_{q0}\Delta i_F + \frac{p}{J_t}\left(\frac{1}{2\pi n_0}\Delta P_m - \frac{P_{m0}}{2\pi n_0^2}\Delta n\right) \end{aligned} \tag{11}$$

Combining the state equations (10) and (11), the state-space representation of the turbine-alternator sub-system is obtained in the form:

$$\begin{pmatrix} \frac{d\Delta i_d}{dt} \\ \frac{d\Delta i_q}{dt} \\ \frac{d\Delta i_F}{dt} \\ \frac{d\Delta \delta_p}{dt} \\ \frac{d\Delta n}{dt} \end{pmatrix} = [A_{TG}] \cdot \begin{pmatrix} \Delta i_d \\ \Delta i_q \\ \Delta i_F \\ \Delta \delta_p \\ \Delta n \end{pmatrix} + [B_{TG}] \cdot \begin{pmatrix} \Delta U \\ \Delta u_F \\ \Delta P_m \end{pmatrix} \tag{12}$$

where the system matrices $[A_{TG}]$ and $[B_{TG}]$ are given in appendix 1.

3.1.4 Model of the Hydraulic Turbine

The water gate opening Y and the head H_f have a direct influence on the water velocity in the penstock and thus on the flow rate. In stability studies of power systems, if mechanical power P_m is the output variable and gate opening Y the input variable, the non ideal hydraulic turbine can be represented by a transfer function F_{TH} as follows [3], [15] :

$$F_{TH}(s) = K_t \frac{1 + b_{th1} T_w s}{1 + a_{th1} T_w s} \tag{13}$$

where,

s= Laplace operator
T_W= hydraulic time constant for a given load level
K_t= gain of hydraulic turbine
a_{th1} and b_{th1}= coefficients of transfer function

The canonical state-space representation for small variations about a stable operating point, derived from the function (13) is of the form:

$$\frac{dx_t}{dt} = -\frac{1}{a_{th1}T_w}x_t + \frac{1}{a_{th1}T_w}\Delta y$$
$$\Delta P_m = K_t\left(1 - \frac{b_{th1}}{a_{th1}}\right)x_t + \frac{K_t b_{th1}}{a_{th1}}\Delta y \quad (14)$$

where the coefficients of the state-space model are represented in Appendix 2.

3.2 State-Space Models of the Control Systems

As shown in fig. 1, there are three control loops in the system –the flow, the speed and the voltage control systems.

3.2.1 The Flow Control System

The block diagram of the flow control system [16] is shown in fig. 2.

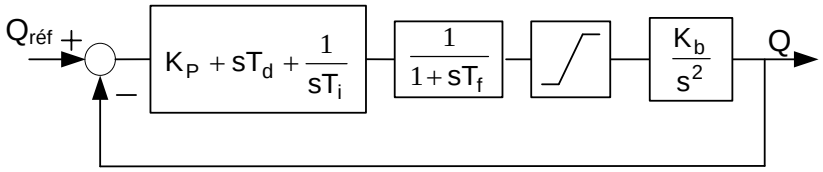

FIG. 2 : BLOCK DIAGRAM OF THE FLOW CONTROL SYSTEM

The system incorporates a PID controller. The variables and parameters in the block diagram are defined as follows:

Q = water flow rate
$Q_{réf}$ = reference water flow rate
K_P = proportional gain of the PID flow controller
T_d = rate time of the PID flow controller
T_i = reset time of the PID flow controller
T_f = filter time constant of the flow-head converter
K_b = rate of slope

The closed-loop transfer function of the system is of the form:

$$F_{RB}(s) = \frac{b_{0rb} + b_{1rb}s + b_{2rb}s^2}{a_{0rb} + a_{1rb}s + a_{2rb}s^2 + a_{3rb}s^3 + s^4} \quad (15)$$

where the coefficients a_{irb} and b_{irb} are represented in Appendix 3. The corresponding canonical controllable state-space representation is of the form:

$$\begin{pmatrix} \frac{dx_{rb1}}{dt} \\ \frac{dx_{rb2}}{dt} \\ \frac{dx_{rb3}}{dt} \\ \frac{dx_{rb4}}{dt} \end{pmatrix} = \begin{bmatrix} 0 & 1 & 0 & 0 \\ 0 & 0 & 1 & 0 \\ 0 & 0 & 0 & 1 \\ -a_{0rb} & -a_{1rb} & -a_{2rb} & -a_{3rb} \end{bmatrix} \begin{pmatrix} x_{rb1} \\ x_{rb2} \\ x_{rb3} \\ x_{rb4} \end{pmatrix} + \begin{bmatrix} 0 \\ 0 \\ 0 \\ 1 \end{bmatrix} \Delta Q_{réf} \quad (16)$$

$$\Delta Q = \begin{bmatrix} b_{0rb} & b_{1rb} & b_{2rb} & 0 \end{bmatrix} \begin{pmatrix} x_{rb1} \\ x_{rb2} \\ x_{rb3} \\ x_{rb4} \end{pmatrix}$$

3.2.2 The Speed Control System

The block diagram of the speed control system is shown in fig. 3 [3], [17]. The system incorporates a PI controller.

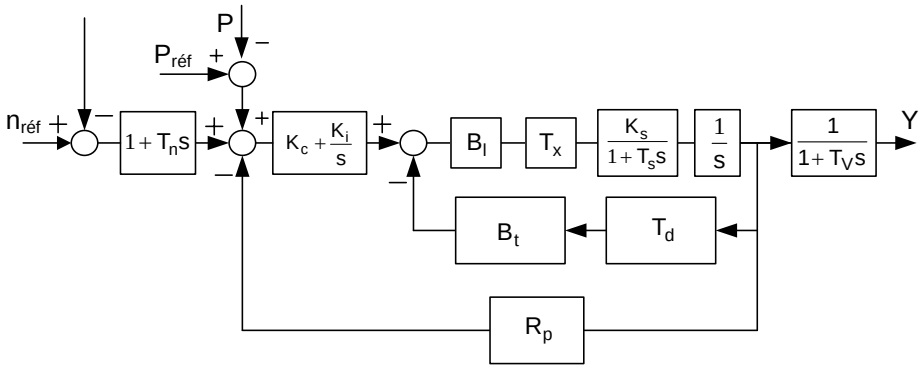

FIG. 3: SPEED CONTROL SYSTEM

The variables and parameters in the block diagram are defined as follows:

Y: Water gate opening

n: Angular speed of the alternator

P: Active power supplied to the load by the alternator

$n_{réf}$: Speed set point

$P_{réf}$: Active power set point

T_n : Time constant

K_c : Proportional gain of PI

K_i : Integral gain of PI Controller

B_l : gain of limiter

T_x : Time constant

K_s : Gain of the servo valve

T_s and T_V : Time constants of the servo valve and valve-wagon units respectively

B_t : Transient droop

R_p: Permanent droop

T_d : Minor loop Time constant

In addition to the main speed control feedback loop, a subsidiary power feedback loop is applied to the system to limit the active power supplied during transient operation or in situations of overload.

The closed-loop transfer function of the system is of the form:

$$Y = \frac{b_{0rv} + b_{1rvn}s + b_{2rvn}s^2}{a_{0rv} + a_{1rv}s + a_{2rv}s^2 + a_{3rv}s^3 + s^4}\left(N_{réf} - N\right) + \frac{b_{0rv} + b_{1rvp}s}{a_{0rv} + a_{1rv}s + a_{2rv}s^2 + a_{3rv}s^3 + s^4}\left(P_{réf} - P\right) \qquad (17)$$

where the coefficients a_{irv}, b_{irvn} and b_{irvp} are represented in Appendix 4. The canonical state-space representation, derived from the closed-loop transfer function, is of the form:

$$\begin{pmatrix} \frac{dx_{rv1}}{dt} \\ \frac{dx_{rv2}}{dt} \\ \frac{dx_{rv3}}{dt} \\ \frac{dx_{rv4}}{dt} \\ \frac{dx'_{rv1}}{dt} \\ \frac{dx'_{rv2}}{dt} \\ \frac{dx'_{rv3}}{dt} \\ \frac{dx'_{rv4}}{dt} \end{pmatrix} = \begin{bmatrix} 0 & 1 & 0 & 0 & 0 & 0 & 0 & 0 \\ 0 & 0 & 1 & 0 & 0 & 0 & 0 & 0 \\ 0 & 0 & 0 & 1 & 0 & 0 & 0 & 0 \\ -a_{0rv} & -a_{1rv} & -a_{2rv} & -a_{3rv} & 0 & 0 & 0 & 0 \\ 0 & 0 & 0 & 0 & 0 & 1 & 0 & 0 \\ 0 & 0 & 0 & 0 & 0 & 0 & 1 & 0 \\ 0 & 0 & 0 & 0 & 0 & 0 & 0 & 1 \\ 0 & 0 & 0 & 0 & -a_{0rv} & -a_{1rv} & -a_{2rv} & -a_{3rv} \end{bmatrix} \begin{pmatrix} x_{rv1} \\ x_{rv2} \\ x_{rv3} \\ x_{rv4} \\ x'_{rv1} \\ x'_{rv2} \\ x'_{rv3} \\ x'_{rv4} \end{pmatrix} + \begin{bmatrix} 0 & 0 \\ 0 & 0 \\ 0 & 0 \\ 1 & 0 \\ 0 & 0 \\ 0 & 0 \\ 0 & 0 \\ 0 & 1 \end{bmatrix} \begin{pmatrix} \Delta P_{réf} - \Delta P \\ \Delta n_{réf} - \Delta n \end{pmatrix}$$

$$\Delta Y = \begin{bmatrix} b_{0rv} & b_{1rvp} & 0 & 0 & b_{0rv} & b_{1rvn} & b_{2rvn} & 0 \end{bmatrix} \begin{pmatrix} x_{rv1} \\ x_{rv2} \\ x_{rv3} \\ x_{rv4} \\ x'_{rv1} \\ x'_{rv2} \\ x'_{rv3} \\ x'_{rv4} \end{pmatrix} \tag{18}$$

3.2.3 The Voltage Regulator

The block diagram of the voltage regulator is shown in fig. 4.

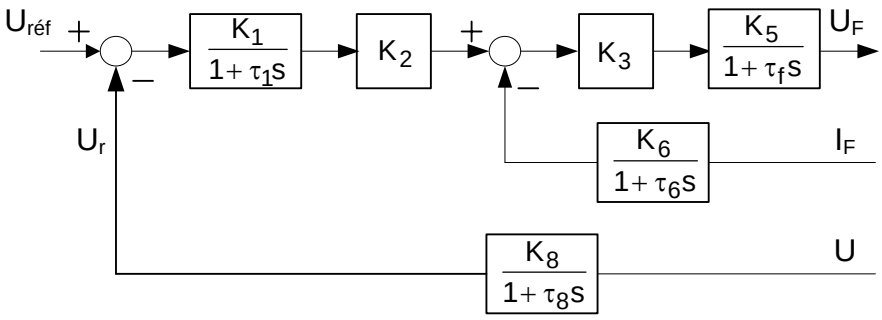

FIG. 4 : BLOCK DIAGRAM OF THE VOLTAGE CONTROL LOOP

The parameters in the block diagram are defined as follows:

$U_{réf}$: Armature voltage set point
U : RMS value of armature voltages
I_F : Excitation current
U_F : Excitation voltage
U_r : Voltage representing the RMS value of Armature coils voltages
K_1 : Gain of the voltage regulator
τ_1 : Time constant of the voltage regulator
K_2 : Gain of the reference voltage amplifier
K_3 : Slope of the thyristor characteristic
K_5 : Gain of the excitation voltage regulator
τ_f : Time constant of the excitation voltage
K_6 : Gain of the current regulator
τ_6 : Time Constant of the current regulator

K_8 : Conductance of the armature voltage control chain
τ_8 : Time constant of the armature voltage control chain

The canonical state-space representation, derived from the closed-loop transfer function is of the form:

$$\begin{pmatrix} \frac{dx_{rt1}}{dt} \\ \frac{dx_{rt2}}{dt} \\ \frac{dx_{rt3}}{dt} \\ \frac{dx_{rt4}}{dt} \end{pmatrix} = \begin{bmatrix} -a_{0rt} & -a_{1rt} & -a_{2rt} & 0 \\ 0 & -a_{3rt} & 0 & 0 \\ 0 & 0 & -a_{4rt} & -a_{5rt} \\ 0 & 0 & 0 & -a_{6rt} \end{bmatrix} \begin{pmatrix} x_{rt1} \\ x_{rt2} \\ x_{rt3} \\ x_{rt4} \end{pmatrix} + \begin{bmatrix} 0 & 0 & 0 \\ 1 & 0 & 0 \\ 0 & 1 & 0 \\ 0 & 0 & 1 \end{bmatrix} \begin{pmatrix} \Delta i_F \\ \Delta U_{réf} \\ \Delta U \end{pmatrix} \tag{19}$$

$$\Delta u_F = b_{rt}\ x_{rt1}$$

where the coefficients a_{irt} and b_{rt} are represented in Appendix 5.

3.2.4 The Power System Load

The behavior of the power system load has great influence on its stability and that of the generating units. The multiplicity of loads and the diversity of their behavior make their modeling a difficult task. Traditionally, load models are classified in two broad categories: static and dynamic loads. Here we consider static loads whose voltage-frequency behavior can be described by exponential equations [3], [15] of the forms:

$$\begin{aligned} P_L &= P_{L0}\left(\frac{U}{U_0}\right)^m \left(1 + K_{pf}\,\Delta f\right) \\ Q_L &= Q_{L0}\left(\frac{U}{U_0}\right)^n \left(1 + K_{qf}\,\Delta f\right) \end{aligned} \tag{20}$$

where :

P_{L0} = initial value of active power in pu
Q_{L0} = initial value of reactive power in pu
U_0 = initial RMS value of armature voltages in pu
U = RMS value of generator armature voltages in pu
Δf = variation of the frequency in pu
m, n = voltage exponent for active and reactive loads respectively
K_{pf} = frequency sensitivity for active load
K_{qf} = frequency sensitivity for reactive load

The linearized version of equations (20) is then:

$$\begin{aligned} \Delta P_L &= \frac{mP_{L0}}{U_0}\Delta U + P_{L0}K_{pf}\,\Delta f \\ \Delta Q_L &= \frac{nQ_{L0}}{U_0}\Delta U + Q_{L0}K_{qf}\,\Delta f \end{aligned} \tag{21}$$

The small variation of the RMS value of the armature voltages in the reference frame of the alternator is of the form :

$$\Delta U = R_d\Delta i_d + R_q\Delta i_q + U_\delta\Delta\delta_p + U_f\Delta f \tag{22}$$

where the coefficients R_d, R_q, U_δ and U_f are represented in Appendix 6.

3.3 State-Space Model of the Power System

Combining the models of the constituent sub-systems, we obtain an 18^{th} order state-space model of the power system that is of the form:

$$\frac{d}{dt}(\Delta x) = [A_S](\Delta x) + [B_S]\begin{pmatrix} \Delta P_{réf} \\ \Delta n_{réf} \\ \Delta U_{réf} \end{pmatrix} \qquad (23)$$
$$(\Delta y) = [C_S]\ (\Delta x)$$

where,

(Δx) = 18x1 state vector

(Δy) = 13x1 output vector

$[A_S]$ = 18x18 matrix (the A-matrix)

$[B_S]$ = 18x3 matrix (the B-matrix)

$[C_S]$ = 13x18 matrix (the C-matrix)

The elements of these different matrices and vectors are presented in Appendix 7.

IV. SIMULATION RESULTS AND DISCUSSION

In this paper, to show the validity of the linearized state-space model of the Cameroonian SIG, and hence to investigate the performance of its PID controller, PID controlled voltage and speed regulators, simulation works have been carried out for the single machine system connected to a load, using MATLAB programs designed by the authors. Most of the model parameters used in the ensuing simulation are given in the appendix and were obtained from technical manuals of the system. Some parameters were obtained from experiments on a prototypal alternator [18].

In order to prove the validity of the model, the results are compared with those given in source books like [3] and [15]. The perturbations considered in this paper are input unit steps which are applied to the system. We consider the operating point given in appendix 8 which also gives the values of sub-systems parameters. The parameterized state-space model is presented in Appendix 7. The simulation results are step responses of water flow deviation, armature voltage deviation, rotor speed deviation and rotor angle deviation. They are depicted respectively in figures 5 to 8.

Fig. 5 illustrates the step response of the dam water flow system given in fig.2, to a unit step disturbance of the reference water flow rate.

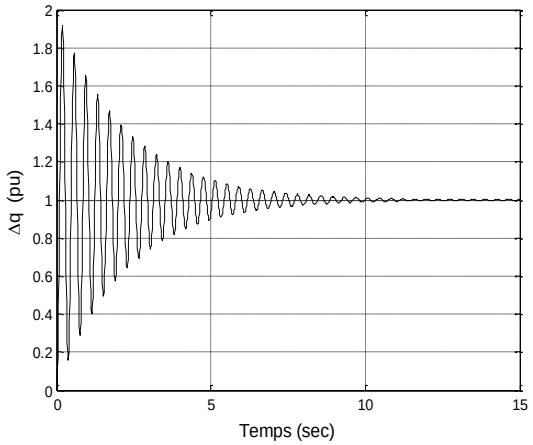

FIG. 5 : RESPONSE TO THE SET POINT UNIT STEP OF THE WATER FLOW

The PID controller really stabilizes the system. The dynamics of the water flow rate deviation exhibits during post perturbation state many oscillations with large initial amplitude which then decreases slowly, before it settles to its steady state value 1,0. The system is poorly damped and it is not regulated back to zero deviation after a unit step perturbation of the water flow set point. The system with classical PID controller has a long settling time and a bad accuracy.

Fig. 6 illustrates the step responses of the turbine-alternator system, following a disturbance of the reference armature voltage. It shows the deviations of the armature voltage ΔU, the rotor speed Δn and the polar wheel angle $\Delta\delta_p$.

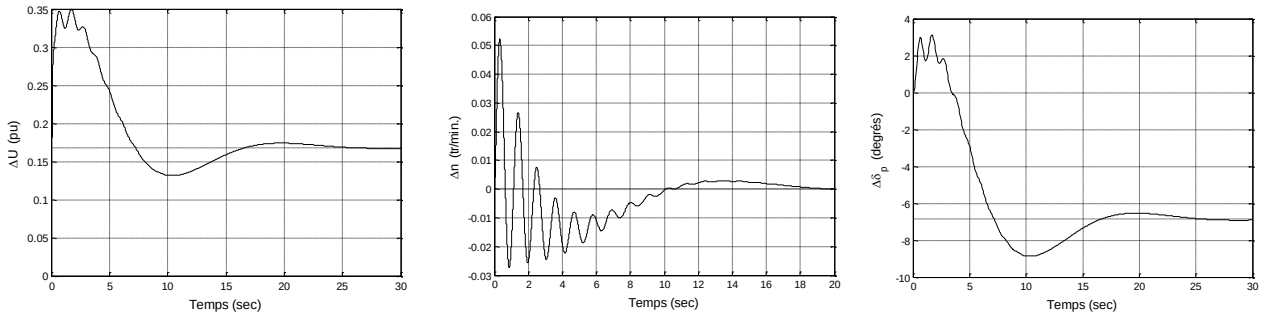

FIG. 6: RESPONSES TO THE SET POINT UNIT STEP OF THE ARMATURE VOLTAGE

The dynamics of the armature voltage deviation exhibits a first swing with overshoot during post perturbation state, before it decreases, oscillates slowly and settles to its non zero steady state value; it contains high frequencies due to transients in stator voltages. The PID controlled AVR really stabilizes the system, but not accurately; the armature voltage perturbation is poorly damped and not regulated back to zero by the AVR. The dynamics of the rotor speed deviation displays during post perturbation state, an acceleration of the rotor in the first half cycle and its deceleration in the second half cycle and so on, with decreasing amplitude; it oscillates slowly and settles to its zero steady state value; the perturbation is completely cleared by the speed controller. The dynamics of the rotor angle deviation exhibits during post perturbation state a first positive swing followed by a negative swing, before it oscillates slowly after a negative overshoot and settles to its non zero steady state value.

Fig. 7 illustrates the step responses of the turbine-alternator system, following a disturbance of the reference rotor speed. It shows the deviations of the rotor speed Δn, the rotor angle $\Delta\delta_p$ and the armature voltage ΔU.

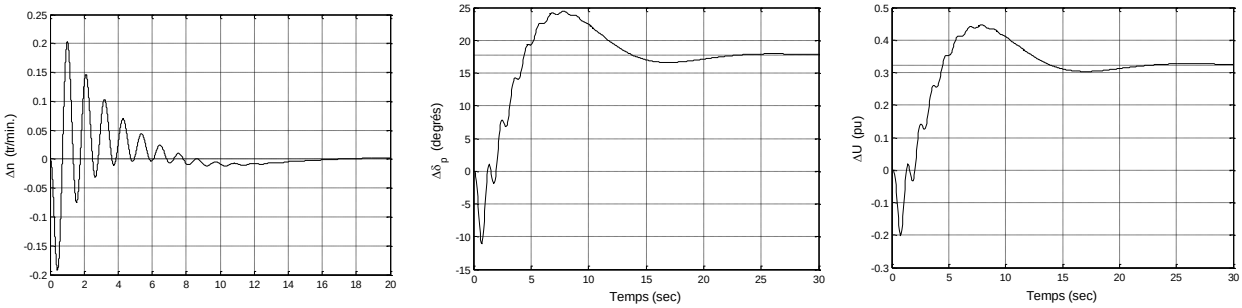

FIG. 7 : RESPONSES TO THE SET POINT UNIT STEP OF THE ROTOR SPEED

The dynamics of the rotor speed deviation exhibits during post perturbation state, first a decrease followed by an increase and oscillations with decreasing amplitude, before it settles to its zero steady state value; the perturbation is completely cleared by the speed controller. The rotor is decelerated in the first half cycle and accelerated in the second half cycle and so on, with decreasing amplitude; it oscillates slowly and settles to its zero steady state value. The PID controlled speed regulator really stabilizes the system, accurately. The rotor angle deviation first exhibits a decrease and then it increases steadily to reach a positive overshoot; it then decreases and oscillates to stabilize at a non zero value. The armature voltage deviation first exhibits a decrease and then it increases steadily to reach a positive peak value and decreases to stabilize at a non zero value. The PID controlled AVR really stabilizes the system, but not accurately. The initial retardation of the rotor has an aftereffect on the rotor angle and the armature voltage. They are caused by high frequency transients in the transformer voltage terms in the stator voltages.

Fig. 8 illustrates the step responses of the turbine-alternator system, following a disturbance of the reference active power demand. It shows the deviations of the rotor speed Δn, the polar wheel angle $\Delta\delta_p$ and the RMS value of the armature voltages ΔU.

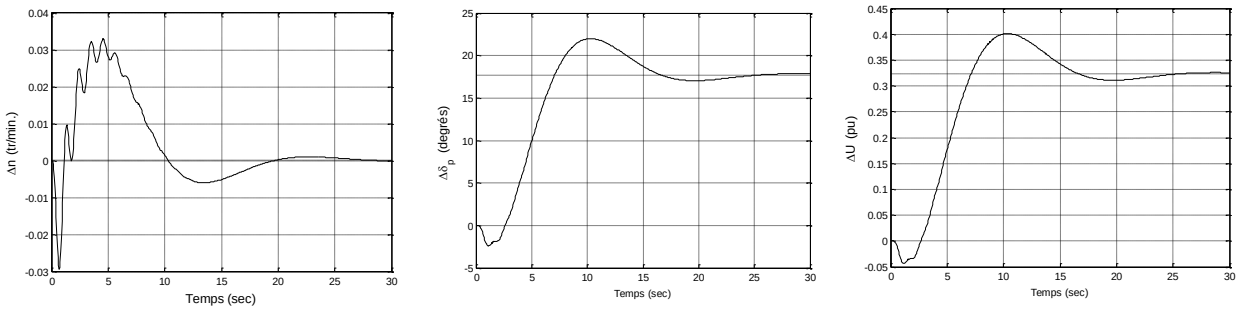

FIG. 8 : RESPONSES TO THE SET POINT UNIT STEP OF THE ACTIVE POWER DEMAND

The dynamics of the rotor speed deviation exhibits during post perturbation state a high negative peak that means a sharp deceleration in the first half cycle, followed by an acceleration in the second half cycle and so on; it increases to a high positive overshoot and then decreases and oscillates around zero, before it settles to its zero steady state value; the power perturbation is completely cleared by the speed controller: the PID controlled speed regulator really stabilizes the system, accurately. The dynamics of the rotor angle deviation and the armature voltage deviation exhibit a first decrease to negative values (backswing phenomenon) and then a steady increase to positive values. They exhibit overshoots and stabilize at non zero values. The PID controlled regulator does not clear the perturbation of the power demand.

The high frequency oscillations affecting the rotor speed are due to the derivative action of the rotating mechanical system of the turbine-alternator system.

V. CONCLUSION

A linearized dynamic model of the Cameroonian southern grid has been developed, using the state-space approach. The model is modular in structure. Intensive MATLAB simulation has been carried out to investigate the behavior of the southern grid of the Cameroon power system, after small disturbances. The simulation results have shown that classical controllers actually in the southern grid of the Cameroon power system ensure stability of the SIG, but they are not accurate, they are slow. The power system is poorly damped. This assessment can serve as a basis for the design of most efficient additional automatic controls to operate in combination with classical controllers present in the SIG.

REFERENCES

[1] **Kundur P., Morison G.K.**, « A Review of Definitions and Classification of Stability Problems in Today's Power Systems », Proc. of IEEE PES Meeting, New York, 2-6 February 1997.

[2] **Graham Rogers**, « Power System Oscillations », Kluwer Academic Publishers, 2002.

[3] **Kundur P**., « Power System Stability and Control », McGraw-Hill, Inc., 1994.

[4] **Demello F.P., C. Concordia**, « Concepts of synchronous machine stability as affected by excitation control », IEEE Trans. PAS, PAS-88, pp.316-329, 1969.

[5] **Jan Machowski, Janusz W. Bialek, James R. Bumby**, « Power System Dynamics: Stability and Control », John Wiley & Sons, Ltd, second edition 2008, ISBN 978-0-470-72558-0.

[6] **PA. Government Services Inc.**, « PEAC » Première Etude du Schéma Directeur pour l'Afrique Centrale, Mai 2005, pp3.18-3.23.

[7] **Crappe Michel.**, « Commande et régulation des réseaux électriques : Evolution des réseaux électriques européens face à de nouvelles contraintes et impact de la production décentralisée », Chapitre 2, Traité EGEM, Lavoisier 2003, pp 49-99.

[8] **D. Baghani, A. Koochaki,** « Multi-Machine Power System Optimized Fuzzy Stabilizer Designe by Using Cuckoo Search Algorithm », International Electrical Journal (IEEJ), Vol. 7(2016) No.3, pp.2182-2187, ISSN 2078-2365.

[9] **H. Glavitsch,** « Control Of Power Generation And System Control With The Emphasis On Modern Control Theory », *IFAC*, Proc. of *International Conference on Automatic Control in Power Generation Distribution and Protection, Pretoria, South Africa* 1980.

[10] **M. Ouassaid, A. Nejmi, M. Cherkaoui, and M. Maaroufi,** « A New Nonlinear Excitation Controller for Transient Stability Enhancement in Power Systems », Proc. of World Academy of Science, Engineering And Technology Volume 8 October 2005 ISSN 1307-6884.

[11] **Kundur P., Klein M., Rogers G. J., and Zywno M. S.**, "Application of Power System Stabilizers for Enhancement of overall System Stability", IEEE Transactions on Power Systems, Vol. 4, 1989, pp. 614-626.

[12] **Chow J. H., Sanchez-Gasca J. J.**, « Pole-placement Designs of Power System Stabilizers », IEEE Transactions on Power Systems , Vol. 4, No.1, 1989, pp. 271-277.

[13] **Pedro Camilo de Oliveira e Silva, Basile Kawkabani, Sébastien Alligné, Christophe Nicolet, Jean-jacques Simond, and François Avellan**, « Stability Study on Hydroelectric Production Site Using Eigenvalues Analysis Method », Journal of Energy and Power Engineering, Vol. 6, 2012, pp. 940-948.

[14] **J. H. TSOCHOUNIE**, « Commande Multivariable du Réseau Interconnecté Sud du Cameroun dans l'Espace d'Etat », Ph.D/Doctoral thesis in Electrical Engineering, National Polytechnic Institute, Yaounde, Cameroon, 2008..

[15] **Padiyar K. R.**, « Power System Dynamics : Stability and Control », John Wiley & Sons (Asia) Pte Ltd, 1996.

[16] **GEC ALSTHOM**, « Automate d'aménagement : Analyse procédé », Aménagement hydroélectrique de SongLoulou, 1999.

[17] **V. Raeber et L. Bonny**, « Régleur électronique », Bulletin technique VEVEY, 1962.

[18] **Barret Jean-Paul, Bornard Pierre, Meyer Bruno**, « Simulation des réseaux électriques », Editions Eyrolles 1997.

APPENDIX

Appendix 1: Matrices of Generator and Turbine-Generator Unit Models.

$\left[A'_G\right]=\left[L_G\right]^{-1}\cdot\left[R_G\right]$ and $\left[B'_G\right]=\left[L_G\right]^{-1}$

where,

$$\left[L_G\right]=\begin{bmatrix} L_d & 0 & \sqrt{\frac{3}{2}}M_{FS} & \sqrt{\frac{3}{2}}M_{KD,S} & 0 \\ 0 & L_q & 0 & 0 & \sqrt{\frac{3}{2}}M_{KQ,S} \\ \sqrt{\frac{3}{2}}M_{FS} & 0 & L_F & M_{F,KD} & 0 \\ \sqrt{\frac{3}{2}}M_{KD,S} & 0 & M_{F,KD} & L_{KD} & 0 \\ 0 & \sqrt{\frac{3}{2}}M_{KQ,S} & 0 & 0 & L_{KQ} \end{bmatrix} \quad \left[R_G\right]=\begin{bmatrix} -R_1 & -\dot{\theta}L_q & 0 & 0 & -\sqrt{\frac{3}{2}}\dot{\theta}M_{KQ,S} \\ \dot{\theta}L_d & -R_1 & \sqrt{\frac{3}{2}}\dot{\theta}M_{FS} & \sqrt{\frac{3}{2}}\dot{\theta}M_{KD,S} & 0 \\ 0 & \sqrt{\frac{3}{2}}\dot{\theta}M_{FS} & -R_F & 0 & 0 \\ 0 & \sqrt{\frac{3}{2}}\dot{\theta}M_{KD,S} & 0 & -R_{KD} & 0 \\ -\sqrt{\frac{3}{2}}\dot{\theta}M_{KQ,S} & 0 & 0 & 0 & -R_{KQ} \end{bmatrix}$$

L_d = inductance of the imaginary coil in the d-axis
L_q = inductance of the imaginary coil in the q-axis
L_F= inductance of the inductor coil **F**
L_{KD} = inductance of the damping coil **KD**
L_{KQ} = inductance of the damping coil **KQ**
M_{FS} = maximum mutual inductance between the inductor coil **F** and the stator coils
$M_{KD,S}$ = maximum mutual inductance between the damping coil **KD** and the stator coils
$M_{KQ,S}$ =maximum mutual inductance between the damping coil **KQ** and the stator coils
$M_{F,KD}$ = maximum mutual inductance between the inductor coil **F** and the damping coil **KD**

$$\left[A_G\right]=\begin{bmatrix} \frac{-R_1L_F}{L_dL_F-\frac{3}{2}M_{FS}^2} & \frac{-\omega_0L_qL_F}{L_dL_F-\frac{3}{2}M_{FS}^2} & \frac{R_F\sqrt{\frac{3}{2}}M_{FS}}{L_dL_F-\frac{3}{2}M_{FS}^2} \\ \frac{\omega_0L_d}{L_q} & \frac{-R_1}{L_q} & \frac{\sqrt{\frac{3}{2}}\omega_0M_{FS}}{L_q} \\ \frac{R_s\sqrt{\frac{3}{2}}M_{FS}}{L_dL_F-\frac{3}{2}M_{FS}^2} & \frac{\sqrt{\frac{3}{2}}\omega_0M_{FS}L_q}{L_dL_F-\frac{3}{2}M_{FS}^2} & \frac{-R_FL_d}{L_dL_F-\frac{3}{2}M_{FS}^2} \end{bmatrix} \quad \left[B_G\right]=\begin{bmatrix} \frac{L_F\sin\delta_{p0}}{L_dL_F-\frac{3}{2}M_{FS}^2} & \frac{L_FU_0\cos\delta_{p0}}{L_dL_F-\frac{3}{2}M_{FS}^2} & \frac{-\sqrt{\frac{3}{2}}M_{FS}}{L_dL_F-\frac{3}{2}M_{FS}^2} \\ \frac{-\cos\delta_{p0}}{L_q} & \frac{U_0\sin\delta_{p0}}{L_q} & 0 \\ \frac{-\sqrt{\frac{3}{2}}M_{FS}\cos\delta_{p0}}{L_dL_F-\frac{3}{2}M_{FS}^2} & \frac{-\sqrt{\frac{3}{2}}M_{FS}U_0\sin\delta_{p0}}{L_dL_F-\frac{3}{2}M_{FS}^2} & \frac{L_d}{L_dL_F-\frac{3}{2}M_{FS}^2} \end{bmatrix}$$

$$[A_{TG}]=\begin{bmatrix} \frac{-R_1L_F}{L_dL_F-\frac{3}{2}M_{FS}^2} & \frac{-\omega_0L_qL_F}{L_dL_F-\frac{3}{2}M_{FS}^2} & \frac{R_F\sqrt{\frac{3}{2}}M_{FS}}{L_dL_F-\frac{3}{2}M_{FS}^2} & \frac{L_FU_0\cos\delta_{p0}}{L_dL_F-\frac{3}{2}M_{FS}^2} & 0 \\ \frac{\omega_0L_d}{L_q} & \frac{-R_1}{L_q} & \frac{\sqrt{\frac{3}{2}}\omega_0M_{FS}}{L_q} & \frac{U_0\sin\delta_{p0}}{L_q} & 0 \\ \frac{R_1\sqrt{\frac{3}{2}}M_{FS}}{L_dL_F-\frac{3}{2}M_{FS}^2} & \frac{\sqrt{\frac{3}{2}}\omega_0M_{FS}L_q}{L_dL_F-\frac{3}{2}M_{FS}^2} & \frac{-R_FL_d}{L_dL_F-\frac{3}{2}M_{FS}^2} & \frac{-\sqrt{\frac{3}{2}}M_{FS}U_0\sin\delta_{p0}}{L_dL_F-\frac{3}{2}M_{FS}^2} & 0 \\ 0 & 0 & 0 & 0 & p2\pi \\ K_{id} & K_{iq} & K_{iF} & 0 & K_{xg} \end{bmatrix} \quad [B_{TG}]=\begin{bmatrix} \frac{L_F\sin\delta_{p0}}{L_dL_F-\frac{3}{2}M_{FS}^2} & \frac{-\sqrt{\frac{3}{2}}M_{FS}}{L_dL_F-\frac{3}{2}M_{FS}^2} & 0 \\ \frac{-\cos\delta_{p0}}{L_q} & 0 & 0 \\ \frac{-\sqrt{\frac{3}{2}}M_{FS}\cos\delta_{p0}}{L_dL_F-\frac{3}{2}M_{FS}^2} & \frac{L_d}{L_dL_F-\frac{3}{2}M_{FS}^2} & 0 \\ 0 & 0 & 0 \\ 0 & 0 & K_{Pm} \end{bmatrix}$$

Appendix 2: Parameters of Hydraulic Turbine.

Non ideal Hydraulic Turbine: $K_t=1{,}5$; $a_{th13}=1{,}1$;

$a_t=2{,}064\cdot10^{-10}\times P_{L0}+0{,}57$; $a_{th21}=4{,}541\cdot10^{-9}\times P_{L0}+1{,}18$; $b_t=a_t-\frac{a_{th13}\times a_{th21}}{K_t}$.

Coefficients of the state-space model: $a_{0th}=\frac{1}{a_t\cdot T_W}$; $b_{0th}=\frac{K_t}{a_t\cdot T_W}\left(1-\frac{b_t}{a_t}\right)$; $d_{th}=K_t\frac{b_t}{a_t}$

Appendix 3: Coefficients of Transfer Function of Water Flow Control System.

$b_{0rb}=\frac{K_b}{T_fT_i}$; $b_{1rb}=\frac{K_bK_P}{T_f}$; $b_{2rb}=\frac{K_bT_d}{T_f}$; $a_{0rb}=\frac{K_b}{T_fT_i}$; $a_{1rb}=\frac{K_bK_P}{T_f}$; $a_{2rb}=\frac{K_bT_d}{T_f}$; $a_{3rb}=\frac{1}{T_f}$

Appendix 4: Coefficients of Transfer Function of Rotor Speed Control System.

$b_{0rv}=\frac{B_lT_xK_sK_i}{T_sT_v}$; $b_{1rvn}=\frac{B_lT_xK_s(K_c+K_iT_n)}{T_sT_v}$; $b_{12vn}=\frac{B_lT_xK_sK_cT_n}{T_sT_v}$; $b_{1rvp}=\frac{B_lT_xK_sK_c}{T_sT_v}$;

$a_{0rv}=\frac{B_lT_xK_sK_iR_g}{T_sT_v}$; $a_{1rv}=\frac{B_lT_xK_sR_g(R_t+K_c+K_iT_v)}{T_sT_v}$; $a_{2rv}=\frac{1+B_lT_xK_sR_g(R_t+K_c)T_v}{T_sT_v}$; $a_{3rv}=\frac{T_s+T_v}{T_sT_v}$

Appendix 5: Coefficients of Transfer Function of Voltage Control System.

$b_{rt}=\frac{K_3K_5}{\tau_f}$; $a_{0rt}=\frac{1}{\tau_f}$; $a_{1rt}=\frac{K_6}{\tau_6}$; $a_{2rt}=-\frac{K_1K_2}{\tau_1}$; $a_{3rt}=\frac{1}{\tau_6}$; $a_{4rt}=\frac{1}{\tau_1}$; $a_{5rt}=\frac{K_8}{\tau_8}$; $a_{6rt}=\frac{1}{\tau_8}$

Appendix 6: Coefficients of Power System Load Model.

$R_d=\frac{u_{D0}}{U_0}R_{Dd}-\frac{u_{Q0}}{U_0}X_{Qd}$; $R_q=\frac{u_{D0}}{U_0}X_{Dq}+\frac{u_{Q0}}{U_0}R_{Qq}$; $U_\delta=\frac{u_{D0}}{U_0}U_{D\delta}-\frac{u_{Q0}}{U_0}U_{Q\delta}$; $U_f=-\frac{u_{D0}}{U_0}U_{Df}+\frac{u_{Q0}}{U_0}U_{Qf}$

The voltages u_{D0} and u_{Q0}, and the currents i_{D0} and i_{Q0}, are Kron's components of armature voltages v_a, v_b and v_c, and currents i_a, i_b and i_c respectively, in a new coordinate system D, Q and 0. They represent steady-state voltages across and currents in two imaginary coils located on the D and Q axis of the stator, for a given operating point, and are obtained as follows: $\begin{pmatrix} u_D \\ u_Q \\ u_0 \end{pmatrix}=[K(\theta_0)]^{-1}\begin{pmatrix} v_a \\ v_b \\ v_c \end{pmatrix}$ and $\begin{pmatrix} i_D \\ i_Q \\ i_0 \end{pmatrix}=[K(\theta_0)]^{-1}\begin{pmatrix} i_a \\ i_b \\ i_c \end{pmatrix}$

The Kron's transformation matrix $[K(\theta_0)]$ is similar to the Park's.

$$R_{Dd}=\frac{G_{QQ}\cos\delta_{p0}-B_{DQ}\sin\delta_{p0}}{G_{DD}G_{QQ}+G_{DQ}G_{QD}}\ ;\qquad X_{Dq}=\frac{G_{QQ}\sin\delta_{p0}+B_{DQ}\cos\delta_{p0}}{G_{DD}G_{QQ}+G_{DQ}G_{QD}}\ ;\qquad X_{Qd}=\frac{B_{QD}\cos\delta_{p0}+G_{DD}\sin\delta_{p0}}{G_{DD}G_{QQ}+G_{DQ}G_{QD}}\ ;$$

$$R_{Qq}=\frac{-B_{QD}\sin\delta_{p0}+G_{DD}\cos\delta_{p0}}{G_{DD}G_{QQ}+G_{DQ}G_{QD}}\ ;\qquad U_{D\delta}=\frac{G_{QQ}i_{Q0}-B_{DQ}i_{D0}}{G_{DD}G_{QQ}+G_{DQ}G_{QD}}\ ;\qquad U_{Q\delta}=\frac{B_{QD}i_{Q0}+G_{DD}i_{D0}}{G_{DD}G_{QQ}+G_{DQ}G_{QD}}\ ;$$

$$U_{Df}=\frac{G_{QQ}K_{Df}+B_{DQ}K_{Qf}}{G_{DD}G_{QQ}+G_{DQ}G_{QD}}\ ;\qquad U_{Qf}=\frac{B_{QD}K_{Df}-G_{DD}K_{Qf}}{G_{DD}G_{QQ}+G_{DQ}G_{QD}}$$

$$G_{DD}=\frac{P_{L0}}{U_0^2}\left((m-2)\frac{u_{D0}^2}{U_0^2}+1\right)-\frac{Q_{L0}}{U_0^2}\left((n-2)\frac{u_{Q0}u_{D0}}{U_0^2}\right)\ ;\qquad B_{DQ}=\frac{Q_{L0}}{U_0^2}\left((n-2)\frac{u_{Q0}^2}{U_0^2}+1\right)-\frac{P_{L0}}{U_0^2}\left((m-2)\frac{u_{D0}u_{Q0}}{U_0^2}\right)$$

$$B_{QD}=\frac{Q_{L0}}{U_0^2}\left((n-2)\frac{u_{D0}^2}{U_0^2}+1\right)+\frac{P_{L0}}{U_0^2}\left((m-2)\frac{u_{D0}u_{Q0}}{U_0^2}\right)\ ;\qquad G_{QQ}=\frac{P_{L0}}{U_0^2}\left((m-2)\frac{u_{Q0}^2}{U_0^2}+1\right)+\frac{Q_{L0}}{U_0^2}\left((n-2)\frac{u_{Q0}u_{D0}}{U_0^2}\right)$$

$$K_{Df}=\frac{P_{L0}u_{D0}}{U_0^2}K_{pf}-\frac{Q_{L0}u_{Q0}}{U_0^2}K_{qf}\ ;\qquad K_{Qf}=\frac{P_{L0}u_{Q0}}{U_0^2}K_{pf}+\frac{Q_{L0}u_{D0}}{U_0^2}K_{qf}$$

Appendix 7: Parameterized State-space Model and Elements of Model Matrices.

$$A_{1,1}=L_F\omega_b\frac{-R_s+R_d\sin\gamma_0}{L_dL_F-M_{FS}^2}\qquad A_{1,2}=L_F\omega_b\frac{-\omega_{s0}L_q+R_q\sin\gamma_0}{L_dL_F-M_{FS}^2}\qquad A_{1,3}=R_F\omega_b\frac{\sqrt{3/2}\cdot M_{FS}}{L_dL_F-M_{FS}^2}$$

$$A_{1,4}=L_F\omega_b\frac{U_0\cos\gamma_0+U_\delta\sin\gamma_0}{L_dL_F-M_{FS}^2}\qquad A_{1,5}=L_F\omega_b\frac{pU_F\sin\gamma_0}{L_dL_F-M_{FS}^2}\qquad A_{1,15}=-\sqrt{3/2}M_{FS}\omega_b\frac{b_{0RT}}{L_dL_F-M_{FS}^2}$$

$$A_{2,1}=\omega_b\frac{\omega_{s0}L_d-R_q\cos\gamma_0}{L_q}\qquad A_{2,2}=\omega_b\frac{-R_s-R_q\cos\gamma_0}{L_q}\qquad A_{2,3}=\omega_b\frac{\sqrt{3/2}M_{Fs}\omega_{s0}}{L_q}$$

$$A_{2,4}=\omega_b\frac{U_0\sin\gamma_0-U_\delta\cos\gamma_0}{L_q}\qquad A_{2,5}=-\omega_b\frac{pU_F\cos\gamma_0}{L_q}\qquad A_{3,1}=\omega_b\cdot\sqrt{3/2}M_{FS}\frac{R_s-R_d\cos\gamma_0}{L_dL_F-M_{FS}^2}$$

$$A_{3,2}=\omega_b\cdot\sqrt{3/2}M_{FS}\frac{\omega_{s0}L_q-R_q\cos\gamma_0}{L_dL_F-M_{FS}^2}\qquad A_{3,3}=-\omega_b\frac{R_FL_d}{L_dL_F-M_{FS}^2}$$

$$A_{3,4}=\omega_b\cdot\sqrt{3/2}M_{FS}\frac{-U_0\sin\gamma_0-U_\delta\cos\gamma_0}{L_dL_F-M_{FS}^2}\qquad A_{3,5}=-\omega_b\cdot\sqrt{3/2}M_{FS}\frac{pU_F\cos\gamma_0}{L_dL_F-M_{FS}^2}$$

$$A_{3,15}=\omega_b\frac{L_db_{0rt}}{L_dL_F-M_{FS}^2}\qquad A_{4,5}=\omega_b\qquad A_{5,1}=-K_{id}\qquad A_{5,2}=-K_{iq}\qquad A_{5,3}=-K_{iF}$$

$$A_{5,5}=-K_n\qquad A_{5,6}=K_{pm}b_{0TH}\qquad A_{5,7}=K_{pm}d_{TH}b_{01rv}\qquad A_{5,8}=K_{pm}d_{TH}b_{11rv}$$

$$A_{5,11}=K_{pm}d_{TH}b_{02rv}\qquad A_{5,12}=K_{pm}d_{TH}b_{12rv}\qquad A_{5,13}=K_{pm}d_{TH}b_{22rv}\qquad A_{6,6}=-a_{0TH}$$

$$A_{6,7}=b_{01rv}\qquad A_{6,8}=b_{11rv}\qquad A_{6,11}=b_{02rv}\qquad A_{6,12}=b_{12rv}\qquad A_{6,13}=b_{22rv}$$

$$A_{7,8}=1\qquad A_{8,9}=1\qquad A_{9,10}=1\qquad A_{10,1}=-\frac{mP_{L0}R_d}{U_0}\qquad A_{10,2}=-\frac{mP_{L0}R_q}{U_0}$$

$$A_{10,4}=-\frac{mP_{L0}U_\delta}{U_0}\qquad A_{10,7}=-a_{0rv}\qquad A_{10,8}=-a_{1rv}\qquad A_{10,9}=-a_{2rv}\qquad A_{10,10}=-a_{3rv}$$

$A_{11,12}=1$ $A_{12,13}=1$ $A_{13,14}=1$ $A_{14,5}=-1$ $A_{14,11}=-a_{0rv}$ $A_{14,12}=-a_{1rv}$

$A_{14,13}=-a_{2rv}$ $A_{14,14}=-a_{3rv}$ $A_{15,15}=-a_{0rt}$ $A_{15,16}=-a_{1rt}$ $A_{15,17}=-a_{2rt}$

$A_{16,3}=1$ $A_{16,16}=-a_{3rt}$ $A_{17,17}=-a_{4rt}$ $A_{17,18}=-a_{5rt}$ $A_{18,1}=R_d$ $A_{18,2}=R_q$

$A_{18,4}=U_\delta$ $A_{18,5}=pU_f$ $A_{18,18}=-a_{6rt}$

$\omega_{s0}=2\pi f_N$; $\gamma_0=\operatorname{atan}\left(\dfrac{\omega_{S0}L_qI_0\cos\varphi-R_sI_0\sin\varphi}{U_0+R_SI_0\cos\varphi+\omega_{S0}L_qI_0\sin\varphi}\right)$.

$B_{10,1}=1$ $B_{14,2}=1$ $B_{17,3}=1$

$C_{1,1}=1$ $C_{2,2}=1$ $C_{3,1}=R_{Dd}\cos\gamma_0+X_{Qd}\sin\gamma_0$ $C_{3,2}=X_{Dq}\cos\gamma_0-R_{Qq}\sin\gamma_0$

$C_{3,4}=U_{Dd}\cos\gamma_0+U_{Qd}\sin\gamma_0-u_{q0}$ $C_{3,5}=p\left(-U_{Df}\cos\gamma_0-U_{Qf}\sin\gamma_0\right)$

$C_{4,1}=R_{Dd}\sin\gamma_0-X_{Qd}\cos\gamma_0$ $C_{4,2}=X_{Dq}\sin\gamma_0+R_{Qq}\cos\gamma_0$

$C_{4,4}=U_{Dd}\sin\gamma_0-U_{Qd}\cos\gamma_0-u_{q0}$ $C_{4,5}=p\left(-U_{Df}\sin\gamma_0+U_{Qf}\cos\gamma_0\right)$

$C_{5,3}=1$ $C_{6,15}=b_{0rt}$ $C_{7,1}=R_d$ $C_{7,2}=R_q$ $C_{7,4}=U_\delta$ $C_{7,5}=pU_f$

$C_{8,4}=\dfrac{180}{\pi}$ $C_{9,5}=\omega_b\dfrac{60}{p\cdot 2\pi}$ $C_{10,5}=p\cdot f_b$ $C_{11,1}=\dfrac{2}{3}\left(L_d-L_q\right)i_{q0}$

$C_{11,2}=\dfrac{2}{3}\left[\left(L_d-L_q\right)i_{d0}+\sqrt{\dfrac{3}{2}}M_{FS}i_{F0}\right]$ $C_{11,3}=\sqrt{\dfrac{2}{3}}M_{FS}i_{q0}$ $C_{12,1}=\dfrac{mP_{L0}R_d}{U_0}$ $C_{12,2}=\dfrac{mP_{L0}R_q}{U_0}$

$C_{12,4}=\dfrac{mP_{L0}U_\delta}{U_0}$ $C_{12,5}=p\left(\dfrac{mP_{L0}U_f}{U_0}+P_{L0}K_{pf}\right)$ $C_{13,1}=\dfrac{nQ_{L0}R_d}{U_0}$ $C_{13,2}=\dfrac{nQ_{L0}R_q}{U_0}$ $C_{13,4}=\dfrac{nQ_{L0}U_\delta}{U_0}$

$C_{13,5}=p\left(\dfrac{nQ_{L0}U_f}{U_0}+Q_{L0}K_{qf}\right)$ $C_{14,7}=b_{01rv}$ $C_{14,8}=b_{11rv}$ $C_{14,11}=b_{02rv}$ $C_{14,12}=b_{12rv}$ $C_{14,13}=b_{22rv}$

$$[A_S]=\begin{bmatrix}
a_{1,1} & a_{1,2} & a_{1,3} & a_{1,4} & a_{1,5} & 0 & 0 & 0 & 0 & 0 & 0 & 0 & 0 & 0 & a_{1,15} & 0 & 0 & 0\\
a_{2,1} & a_{2,2} & a_{2,3} & a_{2,4} & a_{2,5} & 0 & 0 & 0 & 0 & 0 & 0 & 0 & 0 & 0 & 0 & 0 & 0 & 0\\
a_{3,1} & a_{3,2} & a_{3,3} & a_{3,4} & a_{3,5} & 0 & 0 & 0 & 0 & 0 & 0 & 0 & 0 & 0 & a_{3,15} & 0 & 0 & 0\\
0 & 0 & 0 & 0 & a_{4,5} & 0 & 0 & 0 & 0 & 0 & 0 & 0 & 0 & 0 & 0 & 0 & 0 & 0\\
a_{5,1} & a_{5,2} & a_{5,3} & 0 & a_{5,5} & a_{5,6} & a_{5,7} & a_{5,8} & 0 & 0 & a_{5,11} & a_{5,12} & a_{5,13} & 0 & 0 & 0 & 0 & 0\\
0 & 0 & 0 & 0 & 0 & a_{6,6} & a_{6,7} & a_{6,8} & 0 & 0 & a_{6,11} & a_{6,12} & a_{6,13} & 0 & 0 & 0 & 0 & 0\\
0 & 0 & 0 & 0 & 0 & 0 & 0 & 1 & 0 & 0 & 0 & 0 & 0 & 0 & 0 & 0 & 0 & 0\\
0 & 0 & 0 & 0 & 0 & 0 & 0 & 0 & 1 & 0 & 0 & 0 & 0 & 0 & 0 & 0 & 0 & 0\\
0 & 0 & 0 & 0 & 0 & 0 & 0 & 0 & 0 & 1 & 0 & 0 & 0 & 0 & 0 & 0 & 0 & 0\\
a_{10,1} & a_{10,2} & 0 & a_{10,4} & a_{10,5} & 0 & a_{10,7} & a_{10,8} & a_{10,9} & a_{10,10} & 0 & 0 & 0 & 0 & 0 & 0 & 0 & 0\\
0 & 0 & 0 & 0 & 0 & 0 & 0 & 0 & 0 & 0 & 0 & 1 & 0 & 0 & 0 & 0 & 0 & 0\\
0 & 0 & 0 & 0 & 0 & 0 & 0 & 0 & 0 & 0 & 0 & 0 & 1 & 0 & 0 & 0 & 0 & 0\\
0 & 0 & 0 & 0 & 0 & 0 & 0 & 0 & 0 & 0 & 0 & 0 & 0 & 1 & 0 & 0 & 0 & 0\\
0 & 0 & 0 & 0 & -1 & 0 & 0 & 0 & 0 & 0 & a_{14,11} & a_{14,12} & a_{14,13} & a_{14,14} & 0 & 0 & 0 & 0\\
a_{15,1} & a_{15,2} & 0 & a_{15,4} & a_{15,5} & 0 & 0 & 0 & 0 & 0 & 0 & 0 & 0 & 0 & a_{15,15} & 0 & 0 & 0\\
0 & 0 & 1 & 0 & 0 & 0 & 0 & 0 & 0 & 0 & 0 & 0 & 0 & 0 & 0 & a_{16,16} & 0 & 0\\
0 & 0 & 0 & 0 & 0 & 0 & 0 & 0 & 0 & 0 & 0 & 0 & 0 & 0 & 0 & 0 & a_{17,17} & a_{17,18}\\
a_{18,1} & a_{18,2} & 0 & a_{18,4} & a_{18,5} & 0 & 0 & 0 & 0 & 0 & 0 & 0 & 0 & 0 & 0 & 0 & 0 & a_{18,18}
\end{bmatrix}$$

$$[C_S]=\begin{bmatrix}
1 & 0 & 0 & 0 & 0 & 0 & 0 & 0 & 0 & 0 & 0 & 0 & 0 & 0 & 0 & 0 & 0 & 0\\
0 & 1 & 0 & 0 & 0 & 0 & 0 & 0 & 0 & 0 & 0 & 0 & 0 & 0 & 0 & 0 & 0 & 0\\
c_{3,1} & c_{3,2} & 0 & c_{3,4} & c_{3,5} & 0 & 0 & 0 & 0 & 0 & 0 & 0 & 0 & 0 & 0 & 0 & 0 & 0\\
c_{4,1} & c_{4,2} & 0 & c_{4,4} & c_{4,5} & 0 & 0 & 0 & 0 & 0 & 0 & 0 & 0 & 0 & 0 & 0 & 0 & 0\\
0 & 0 & 1 & 0 & 0 & 0 & 0 & 0 & 0 & 0 & 0 & 0 & 0 & 0 & 0 & 0 & 0 & 0\\
0 & 0 & 0 & 0 & 0 & 0 & 0 & 0 & 0 & 0 & 0 & 0 & 0 & 0 & b_{rt} & 0 & 0 & 0\\
c_{7,1} & c_{7,2} & 0 & c_{7,4} & c_{7,5} & 0 & 0 & 0 & 0 & 0 & 0 & 0 & 0 & 0 & 0 & 0 & 0 & 0\\
0 & 0 & 0 & 1 & 0 & 0 & 0 & 0 & 0 & 0 & 0 & 0 & 0 & 0 & 0 & 0 & 0 & 0\\
0 & 0 & 0 & 0 & c_{9,5} & 0 & 0 & 0 & 0 & 0 & 0 & 0 & 0 & 0 & 0 & 0 & 0 & 0\\
c_{10,1} & c_{10,2} & c_{10,3} & 0 & 0 & 0 & 0 & 0 & 0 & 0 & 0 & 0 & 0 & 0 & 0 & 0 & 0 & 0\\
c_{11,1} & c_{11,2} & 0 & c_{11,4} & c_{11,5} & 0 & 0 & 0 & 0 & 0 & 0 & 0 & 0 & 0 & 0 & 0 & 0 & 0\\
c_{12,1} & c_{12,2} & 0 & c_{12,4} & c_{12,5} & 0 & 0 & 0 & 0 & 0 & 0 & 0 & 0 & 0 & 0 & 0 & 0 & 0\\
0 & 0 & 0 & 0 & 0 & 0 & c_{13,7} & c_{13,8} & 0 & 0 & c_{13,11} & c_{13,12} & c_{13,13} & 0 & 0 & 0 & 0 & 0
\end{bmatrix}$$

$$(\Delta x)=\begin{pmatrix}
\Delta i_d\\ \Delta i_q\\ \Delta i_F\\ \Delta\delta_p\\ \Delta n\\ x_t\\ x_{rv1}\\ x_{rv2}\\ x_{rv3}\\ x_{rv4}\\ x'_{rv1}\\ x'_{rv2}\\ x'_{rv3}\\ x'_{rv4}\\ x_{rt1}\\ x_{rt2}\\ x_{rt3}\\ x_{rt4}
\end{pmatrix}\qquad
[B_S]=\begin{bmatrix}
0 & 0 & 0\\ 0 & 0 & 0\\ 0 & 0 & 0\\ 0 & 0 & 0\\ 0 & 0 & 0\\ 0 & 0 & 0\\ 0 & 0 & 0\\ 0 & 0 & 0\\ 0 & 0 & 0\\ 1 & 0 & 0\\ 0 & 0 & 0\\ 0 & 0 & 0\\ 0 & 0 & 0\\ 0 & 1 & 0\\ 0 & 0 & 0\\ 0 & 0 & 0\\ 0 & 0 & 1\\ 0 & 0 & 0
\end{bmatrix}$$

$$(\Delta y)=\begin{pmatrix}
\Delta i_d\\ \Delta i_q\\ \Delta u_d\\ \Delta u_q\\ \Delta i_F\\ \Delta u_F\\ \Delta U\\ \Delta\delta_p\\ \Delta n\\ \Delta T_{em}\\ \Delta P_L\\ \Delta Q_L\\ \Delta y
\end{pmatrix}\qquad
(\Delta u)=\begin{pmatrix}
\Delta P_{réf}\\ \Delta n_{réf}\\ \Delta U_{réf}
\end{pmatrix}$$

Appendix 8: Values of Parameters of subsystems of State-Space Model.

System Operating Point:

$U_0=1.2247\text{p.u.}$; $P_{L0}=0.9\text{p.u.}$; $Q_{L0}=0.5578\text{p.u.}$; $\cos\varphi_0=0.85$; $I_0=0.7487\text{p.u.}$;

$i_{F0}=1.094\text{p.u.}$; $\eta_{G0}=0.97878$; $n_0=120\text{tr/min.}$; $\delta_{p0}=21°$; $T_w=4.9661\text{sec.}$

Synchronous Generator:

$L_d=1.4938\text{p.u.}$; $L_q=0.9959\text{p.u.}$; $L_\sigma=0.167\text{p.u.}$; $M_{FS}=1.3268\text{p.u.}$; $p=25$

$L_F=1.852\text{p.u.}$; $R_s=0.0152\text{p.u.}$; $R_F=0.0002654\text{p.u.}$, $J_t=8800000\text{kgm}^2$.

Water Flow Control System parameters:

$K_b=50$; $T_f=0{,}916$; $K_p=1$; $T_d=5$; $T_i=10$;

Speed Regulator System parameters:

$n_{ref}=50$; $T_n=2{,}22$; $K_c=2{,}08$; $K_i=0{,}416$; $R_p=1{,}0$; $B_l=0{,}44$; $T_x=1{,}344$; $K_s=0{,}2$; $T_d=2{,}02$; $B_t=0{,}55$; $T_s=0{,}07$; $T_v=0{,}2$.

Voltage Regulator System parameters:

$K_1 = 0{,}1$; $\tau_1 = 0{,}04$; $K_2 = 5{,}39$; $K_3 = 10{,}47$; $K_5 = 1{,}486$; $\tau_f = 0{,}93$; $K_6 = 0{,}971$; $\tau_6 = 0{,}01$;
$K_8 = 0{,}000971$; $\tau_8 = 0{,}01$.

Power System Load:

$m = 2$; $n = 2$; $K_{pf} = 3$; $K_{qf} = -2$.